European Journal of Mechanics / B Fluids 76 (2019) 292–302

Contents lists available at ScienceDirect

European Journal of Mechanics / B Fluids

journal homepage: www.elsevier.com/locate/ejmflu

Revealing electrical stresses acting on the surface of protoplast cells under electric field

Kia Dastani [a,b], Mahdi Moghimi Zand [a,c,d,*], Amin Hadi [a], Changyong Cao [c,d,e,**]

[a] Small Medical Devices, BioMEMS & LoC Lab, Department of Mechanical Engineering, College of Engineering, University of Tehran, Tehran, 14399-55961, Iran
[b] Department of Mechanical Engineering, Sharif University of Technology, 11155-9567, Tehran, Iran
[c] Laboratory of Soft Machines and Electronics, School of Packaging, Michigan State University, East Lansing, MI 48824, USA
[d] Department of Mechanical Engineering, Michigan State University, East Lansing, MI 48824, USA
[e] Department of Electrical and Computer Engineering, Michigan State University, East Lansing, MI 48824, USA

ARTICLE INFO

Article history:
Received 14 August 2018
Received in revised form 3 February 2019
Accepted 25 February 2019
Available online 12 March 2019

Keywords:
Cell engineering
Dielectrophoresis
Microfluidics
Immersed interface method (IIM)
BioMEMS

ABSTRACT

When cells exposed to an electric field, localized changes in the distribution of the electric field will be induced and these changes in turn lead to electrical stresses on cell surface. The electrical stresses play a key role in the cell membrane structural changes which leads to important phenomena like hydrophilic pores formation on the cell membrane resulting in the cell permeability. In this work, protoplast cell interaction with direct current (DC) electric field is investigated. The electrical stresses acted on the cell membrane in the presence of electric field are investigated numerically by a modified finite difference method, fast Immersed Interface Method (IIM). Exact solution of dielectrophoresis (DEP) force applied on a cell under a non-uniform electric field is obtained to verify numerical solution obtained by the fast IIM. The numerical results reveal that both mismatched permittivity between cell and insulating suspension fluid and the applied voltage are essential for generating and tuning the total stresses exerted on cell surface. This paper can help to analytically study the electroporation phenomenon which its exact mechanism is still unclear.

1. Introduction

Significant progresses have been made in mammalian cell engineering over past years for the modification of cellular function such as gene expression [1–8], protein processing [9–12], secretion [13–15], glycosylation [16,17] and proliferation [18–21]. One of the most important aims of cell engineering is to improve the cellular properties of cells for applications in cell therapies and tissue engineering. Electroporation is one of the promising approaches to transfer macromolecule into cell. It allows one to introduce exogenous molecules into cells and simultaneously to extract endogenous molecules from inside of the cells [22]. The formation of hydrophilic pores on the surface of cell membrane makes the cell permeable for achieving this process. The pores are formed by the tension stress exerted on the cell membrane, either mechanically (pipet aspiration) or electrically (electroporation). Up to now, the formation mechanism of the pores caused by electrocompressive stresses has not yet been understood well. It is generally believed that the transmembrane potential reaches a critical value to make cell to rupture. The rupture or irreversible membrane breakdown happens when the pore radius becomes more than a critical value [23]. Membrane rupture mechanism under electric field is also unclear like membrane permeabilization. Electrical stresses should have an important role in both phenomena.

Different theoretical models have been proposed to explain this electroporation phenomenon. The transient aqueous model is one of the most accepted models. It assumed that when cell is exposed to an electric field, the induced transmembrane potential (TMP) provides free energy for phospholipids orientation in the cell membrane, leading to the formation of hydrophilic pores [24–26]. In a previous study, the effect of electric field on cell membrane permeability has been investigated indirectly by measuring the conductivity changes caused by applying electrical pulses and observing molecular transport into cells [27]. TMP depends on cell radius, the electric field intensity, the angle between membrane points and direction of the electric field. It can be calculated by the Schwan's equation [28]. It has been observed that molecule transfection happens more in the part

* Corresponding author at: Small Medical Devices, BioMEMS & LoC Lab, Department of Mechanical Engineering, College of Engineering, University of Tehran, Tehran, 14399-55961, Iran.
** Corresponding author at: Laboratory of Soft Machines and Electronics, School of Packaging, Michigan State University, East Lansing, MI 48824, USA.
E-mail addresses: mahdimoghimi@ut.ac.ir (M. Moghimi Zand), ccao@msu.edu (C. Cao).

https://doi.org/10.1016/j.euromechflu.2019.02.010
0997-7546/

of membrane where TMP is higher. This could be identified by checking the electrical stress distribution acting on the cell surface. Priya and Gowrisree studied the effects of the electric field on the cell in a conductive environment [29]. In their work, TMP was calculated numerically and compared with analytical values, while electroporation was investigated by measuring the TMP. However, in their research, the effect of electric field on the cell was studied only by calculating the potential difference between the inner and outer surface of membrane. In addition, Tekle et al. studied the formation and distribution of pores as well as its lifetime in the cell membrane by applying the electric field [30]. Lysis, a permanent physical rupture of cells plasma membrane, is another important phenomenon when exposure to electric field. The membrane will rupture if the area density of electrical energy reaches certain critical value(typically 5 mJ/m^2) and the transmembrane potential is about 0.5∼1.0 V, depending on the duration of applied field [31]. On the other hand, lysis may also be induced by mechanical stresses. Cell membrane will rupture if the surface tension reaches required value (typically 5 mN/m) [31]. This finding indicates that the mechanism of cell membrane rupture can be studied by monitoring the electrical stresses and strains produced over cell surface in the presence of electric field.

In addition, electro-mechanical permeabilization of lipid vesicles have been investigated by Needham and Hochmuth [32]. They used a micropipette to apply mechanical tension on the cell and studied the effect of mechanical stresses and electrocompressive stresses on cell permeabilization. The critical electric field intensity was provided as a function of mechanical tension on the membrane. However, they did not discuss the effect of the electric field on the cell. Although membrane rupture and pores formation in phospholipid bilayers under the effect of electrical and mechanical stresses have been investigated by molecular dynamics, the mechanism of pores formation in the cell membrane under an electric field is still unclear [33]. In another study, Akinlaja & Sachs reported the combined effects of mechanical and electrical stress on membrane breakdown [34]. It claimed that the mechanism for this membrane breakdown remain unclear. In their experimental research, the effect of electric field on cell membrane was studied indirectly by measuring the conductance and capacitance. The mechanical tension exerted on the membrane was approximated by cell-attached patches from the applied pressure.

As mentioned above, the mechanism of pore formation in the cell membrane when the cell is exposed to an electric field has not been clearly identified. It has mostly been studied indirectly by measurements of conductivity of cell suspensions and cell pellets [35], electro-optical experiments [36] and some other techniques. But the structural changes in the cell membrane in the presence of an electric field have not been studied directly. To better understand the electroporation phenomenon and cell membrane permeability, it was necessary to closely monitor the interaction between cells and electric field. Researchers have examined the dielectrophoretic effect on cells to investigate electroporation phenomena [37]. The effects of dielectrophoresis force in DNA accumulation around the cell membrane has been studied [28]. It has been reported that applying high-voltage electric pulse made the cell membrane permeable while applying lower voltage pulse helped transfer DNA into the cell. Nevertheless, because its dielectric properties were different from insulating suspension fluid, when a cell was exposed to an electric field caused local changes in the electrostatic potential distribution and local non-uniformity in electric field. As a result, electrical stresses were applied on cell surface. The electrical stresses may play a key role in cell membrane structural changes and its permeability which can never be underestimated. These electrical stresses are sometimes known as electrocompressive stresses in literature but depending on cell and insulating suspension fluid dielectric properties, the electrical stress distribution over cell surface is either tensile or compressive.

In this paper, we employ the numerical simulation to study the electrical stresses generated on a cell when it is exposed to an electric. We also discuss the affecting factors that have considerable influence on the distribution and intensity of electrical stresses. Immersed interface method (IIM) is selected and developed to solve the governing equations for this problem based on electrostatic question and the internal boundary conditions, and the electric field is calculated along the outer and inner boundaries of cell membrane. The electric stresses exerted on the cell surface are calculated using Maxwell stress tensor. The model is verified by the numerical results obtained via effective dipole moment (EDM) approach which has been widely used and validated by previous experiments. Specifically, the DEP force induced on a cell that is exposed to a nonuniform electric field is calculated by integrating Maxwell stress tensor over cell surface. However, it is noted that EDM approximation becomes less accurate when the size of cell is not negligible in comparison with the size of device. Thus, to validate the model, the cell radius should be smaller compared to the device size so that the differences between the results become negligible.

2. Theory and governing equations

In a variety of biomedical applications, cells are exposed to electric fields. When an electric field applies on colloidal particles suspended in a fluid, the major electrokinetic phenomena generated include electrophoresis (EP), induced-charge electrophoresis (ICEP) and dielectrophoresis (DEP). When an electric field is applied on cells suspended in a fluid, the most important phenomenon is DEP, which has many applications such as cell trapping, sorting and separating bioparticles [38]. It is known that free and bound bipolar charges are induced at their surfaces due to the Maxwell–Wagner interfacial polarization [39] when cells suspended in an insulating fluid medium are exposed to an external electric field. As a result, interaction of the bipolar charges with electric field induces electrical stresses at cells surfaces which in turn leads to cell deformation.

In this work protoplast electrical model is used to study the behavior of cells in electric field, which has been demonstrated useful in modeling many types of real particles such as biological cells. Protoplasts are prepared by treating cells with special enzymes. Mammalian cells structure and their polarization response in the presence of electric field are similar to protoplasts. Because the applied electric field is direct current or sufficiently low frequency alternating current, the effect of membrane capacitance and transconductance can be neglected. A dielectric lossless cell with permittivity of ε_p, immersed in a fluid with permittivity of ε_f is considered to be exposed to a uniform direct current (DC) electric field. As shown in Fig. 1, the cell is located in a region of a real microfluidic device, where the electric field is uniform. The electrodes and boundary conditions are shown in this figure. The governing equation for the problem can be expressed as below [40]

$$\nabla^2 \varphi = 0 \tag{1}$$

As shown in Fig. 1, the boundary conditions for the problem can be written as

$$\begin{aligned} &\varphi(x, y) = \varphi_1 \qquad \text{at} \quad y = L \\ &\varphi(x, y) = \varphi_2 \qquad \text{at} \quad y = 0 \\ &\frac{\partial \varphi}{\partial x} = 0 \qquad at \quad x = 0 \text{ and } x = L \end{aligned} \tag{2}$$

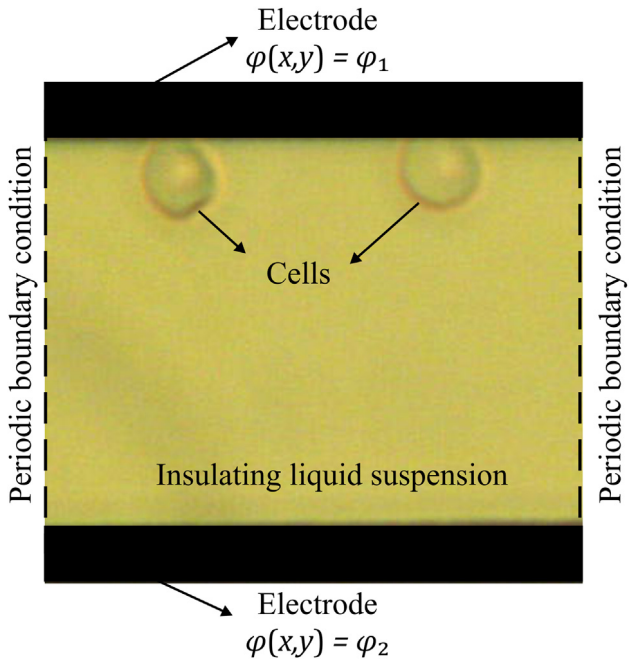

Fig. 1. Geometry and boundary conditions of the model. Cells are immersed in a buffer fluid. Two electrodes are placed on the top and bottom boundary for applying a vertical electric field.

For the dielectric cell without ohmic loss with permittivity of ε_p, immersed in a dielectric fluid with permittivity of ε_f exposed to the DC electric field, the jump conditions along the immersed interface are

$$\varphi_p(x,y) = \varphi_f(x,y)$$
$$\varepsilon_p \frac{\partial \varphi_p}{\partial \vec{n}} = \varepsilon_f \frac{\partial \varphi_f}{\partial \vec{n}} \tag{3}$$

Herein, only the effect of electric field is considered and the magnetic field is ignored, thus Maxwell stress tensor can be expressed as below [41].

$$T_{ij} = \varepsilon \left(E_i E_j - \frac{1}{2} E^2 \delta_{ij} \right) \tag{4}$$

Thus, the electric stress acing on the cell can be calculated as

$$\vec{f} = \varepsilon \left(\vec{E}.\vec{n} \right) \vec{E} - \frac{1}{2} \varepsilon E^2 \vec{n} \tag{5}$$

The electrical stresses on boundary of cell must be calculated both on inner and outer surface. For nomenclature, numbers 1 and 2 denote inner and outer surface of cell membrane respectively. Then according to Eq. (5), we will have

$$\vec{f}_1 = \varepsilon_p \left(\vec{E}_1.\vec{n}_1 \right) \vec{E}_1 - \frac{1}{2} \varepsilon_p {E_1}^2 \vec{n}_1 \tag{6a}$$

$$\vec{f}_2 = \varepsilon_f \left(\vec{E}_2.\vec{n}_2 \right) \vec{E}_2 - \frac{1}{2} \varepsilon_f {E_2}^2 \vec{n}_2 \tag{6b}$$

$$\vec{f} = \vec{f}_1 + \vec{f}_2 \tag{6c}$$

where $\vec{n}_1 = -\vec{n}_2$. It should be noted that since electrical stresses acting over cell surface originate from Maxwell–Wagner interfacial polarization, these electrical stresses have a nonzero time-averaged value while the applied electric field is alternating current. In such condition both bipolar surface charges induced at cell/suspension fluid interface and the applied AC electric field oscillate with the same frequency and the electrical stresses are obtained from the product of two cosine functions [42–44]. Therefore, the time-averaged electrical stresses acting over cell surface will lead to steady state cell deformation when exposed to an AC external electric field.

3. Numerical method and solutions

In the past decades, there are a few numerical methods proposed for solving partial differential equations (PDE) which have irregular boundaries in the solution domain and discontinuous coefficients such as smoothing method [45], harmonic averaging [46], Peskin's immersed boundary (IB) method [47] and immersed interface method (IIM) [48]. In these methods the coefficients of equations are usually discontinuous, i.e., they have jump interface conditions or singular force conditions on the interface. In this work, IIM is employed to solve the interface problem. IIM uses a uniform mesh which makes it easy to handle the geometry and to find and apply the internal boundary conditions on irregular boundary which are known as jump conditions in literature [49]. It uniquely uses a standard 5-point central finite difference scheme at all grid points and only adds a nonzero correction term

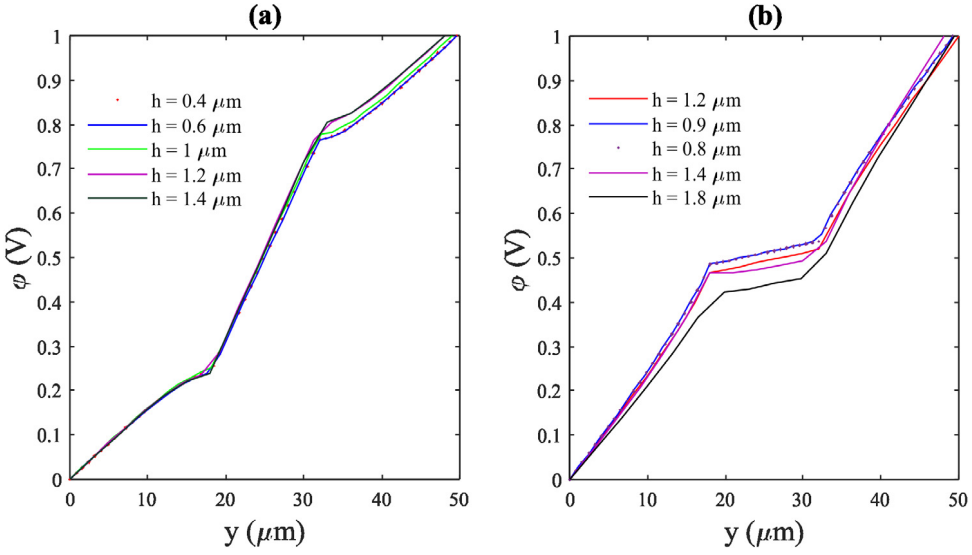

Fig. 2. Electrostatic potential magnitude calculated along the line x = 25 μm for different permittivity ratio of cell and buffer fluid (a) $\varepsilon_p/\varepsilon_f = 0.01$ and (b) $\varepsilon_p/\varepsilon_f = 10$.

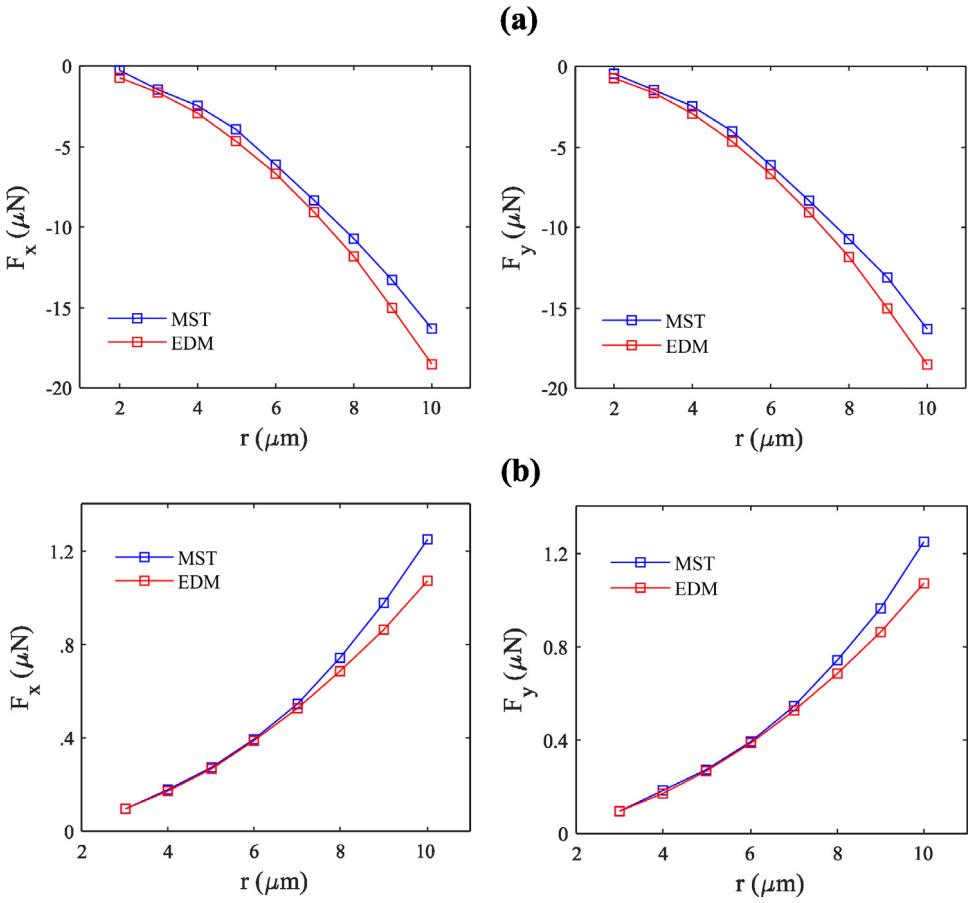

Fig. 3. DEP force as a function of cell ratio. The cell is located at the location of $C_x = 25$ μm and $C_y = 25$ μm. The permittivity ratio of cell and buffer fluid are respectively (a) $\varepsilon_p/\varepsilon_f = 0.2$ and (b) $\varepsilon_p/\varepsilon_f = 50$.

to the right side of the finite difference equations at grid points near or on the interface [48].

In this study, the fast IIM is used for discretization of governing equations due to the constant equation coefficient in two domains. The main idea of fast IIM is weighted least square interpolation. The two-dimensional elliptic differential equation is expressed in Eq. (7a) along with the appropriate boundary conditions on $\partial\Omega$. It is assumed that $\beta(x, y)$ is a constant and is different for each domain.

$$\nabla \cdot (\beta(x, y)\nabla u) = f\ (x, y) \tag{7a}$$

$$\beta\ (x, y) = \begin{cases} \beta^- & if (x, y) \in \Omega^- \\ \beta^+ & if (x, y) \in \Omega^+ \end{cases} \tag{7b}$$

The jump conditions on the cell boundary for the above equations are

$$\left[\beta \frac{\partial u}{\partial n}\right]_\Gamma - \nu = 0 \tag{8a}$$

$$[u]_\Gamma = \omega \tag{8b}$$

The discrete form of Eq. (7a) can be obtained as

$$\sum_k^{n_s} \gamma_k U_{i+i_k, j+j_k} = f_{ij} + C_{ij} \tag{9}$$

When the coefficients for the questions are constant for each domain, or there is a singular force only on the interface, the discrete form of Eq. (7a) can be expressed as follow

$$\Delta_h U_{ij} = \frac{f_{ij}}{\beta_{ij}} + C_{ij} \tag{10}$$

in which Δ_h is the discrete Laplacian operator, and C_{ij} is correction term whose value is zero at regular points. The correction term is calculated at irregular points using Eq. (11), where ω', ν', ω'' and ν'' are first and second order surface derivatives and χ is curvature of the interface.

$$\begin{aligned} C_{ij} = {} & a_2\omega + a_{12}\tfrac{\nu'}{\beta} + \left(a_6 + a_{12}\chi''\right)\omega' + a_{10}\omega'' \\ & + \frac{1}{\beta}\left(a_4 + (a_8 - a_{10})\,\chi''\right)\nu \\ & + a_8\left(\frac{[f]}{\beta} + \frac{\sigma\omega}{\beta} - \omega''\right) \end{aligned} \tag{11}$$

where ω', ν', ω'' and ν'' are first and second order surface derivatives and χ is curvature of the interface. Coefficients a_n are calculated as

$$\begin{aligned} a_1 &= \sum_{k\in K^-} \gamma_k & a_2 &= \sum_{k\in K^+} \gamma_k \\ a_3 &= \sum_{k\in K^-} \xi_k\gamma_k & a_4 &= \sum_{k\in K^+} \xi_k\gamma_k \\ a_5 &= \sum_{k\in K^-} \eta_k\gamma_k & a_6 &= \sum_{k\in K^+} \eta_k\gamma_k \\ a_7 &= \sum_{k\in K^-} \frac{1}{2}\xi_k^2\gamma_k & a_8 &= \sum_{k\in K^+} \frac{1}{2}\xi_k^2\gamma_k \\ a_9 &= \sum_{k\in K^-} \frac{1}{2}\eta_k^2\gamma_k & a_{10} &= \sum_{k\in K^+} \frac{1}{2}\eta_k^2\gamma_k \\ a_{11} &= \sum_{k\in K^-} \xi_k\eta_k\gamma_k & a_{12} &= \sum_{k\in K^+} \xi_k\eta_k\gamma_k \end{aligned} \tag{12}$$

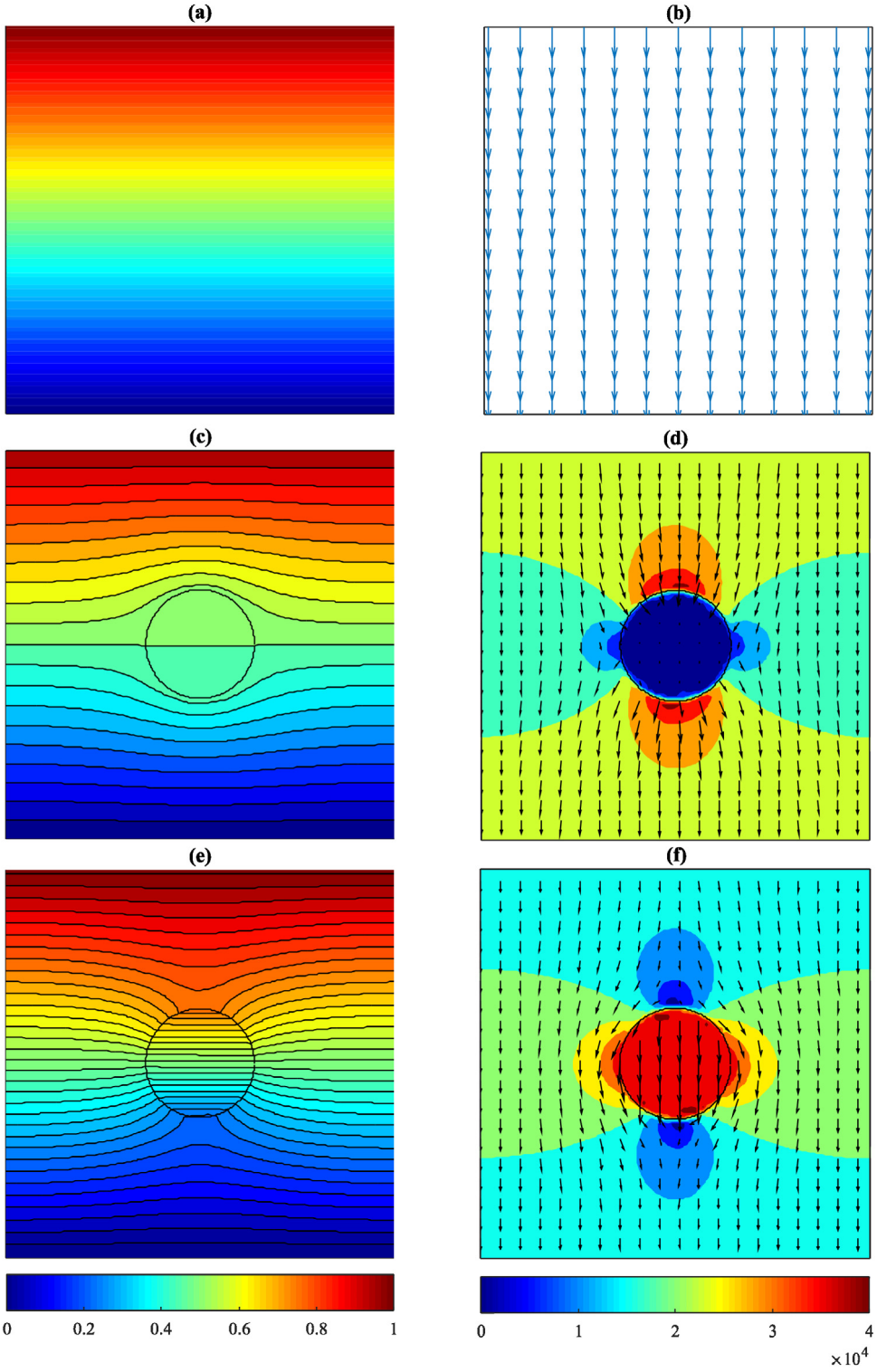

Fig. 4. Effect of cell and its relative permittivity on electrostatic potential distribution (V) and electric field distribution (V/m). (a–b) without cell existing. (c–d) with permittivity ratio $\varepsilon_p/\varepsilon_f = 10$ (e–f) with permittivity ratio $\varepsilon_p/\varepsilon_f = 0.01$. The electrostatic potential and electric field distributions have been distorted by the cell.

where the values *of* γ_k are determined from the applied finite difference stencil, and η_k and ξ_k are local coordinates of the participant points in the finite difference stencils and $K^{\pm} = \{k: (\xi_k, \eta_k)$ is on the $\pm$ side of interface$\}$

We consider augmented variable as $[u_n]_\Gamma = g$. $W = [W_1, W_2, \ldots, W_{n_b}]^T$ and $G = [G_1, G_2, \ldots, G_{n_b}]^T$ are discrete values of g and ω on interface at control points. Since the correction term C_{ij} depends upon values $\{G_k\}$ and $\{W_k\}$, the matrix form of Eq. (10) is obtained as

$$AU + BG = F + B_1 W \equiv F_1 \tag{13}$$

At this point, there is an equation with two unknowns U and G. To determine the second unknown which is G, the jump condition $\left[\beta \frac{\partial u_g}{\partial n}\right]_\Gamma = \nu$ must be discretized. Discrete form of

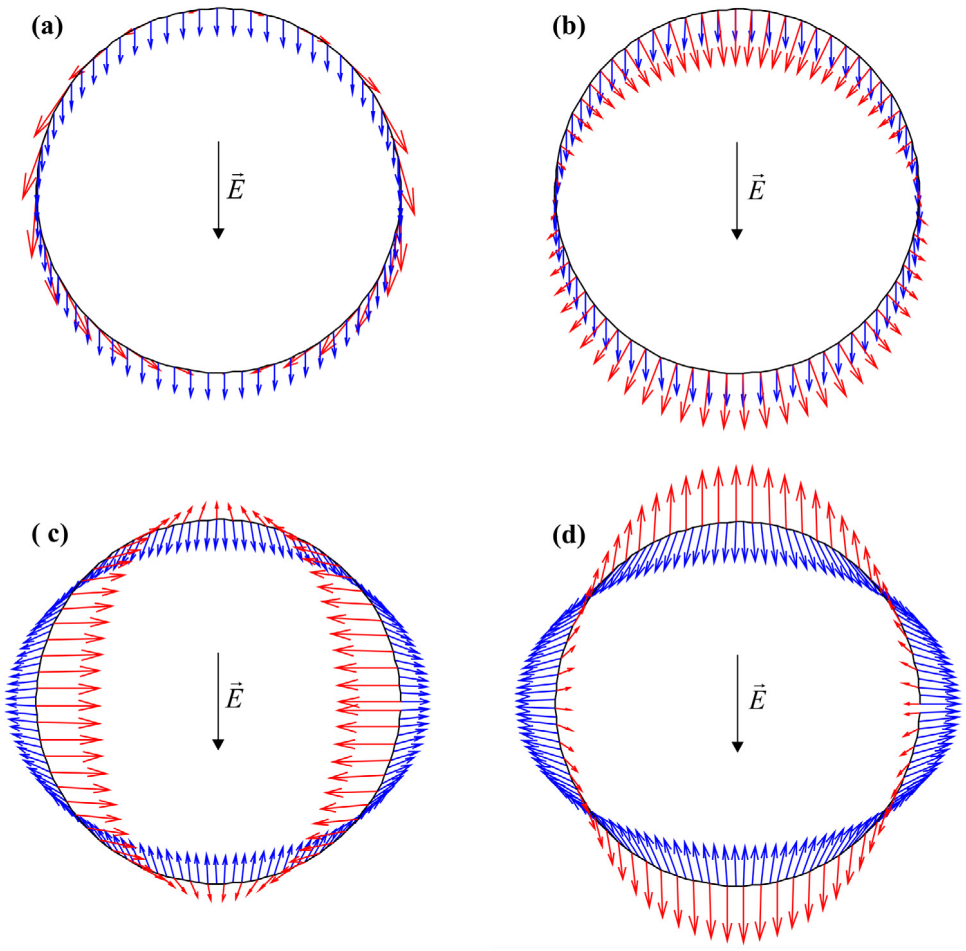

Fig. 5. Electric field on cell surface when the permittivity ratio is (a) $\varepsilon_p/\varepsilon_f < 1$ or (b) $\varepsilon_p/\varepsilon_f > 1$. Electrical stresses generated on inner and outer side of cell membrane when permittivity ratio is (c) $\varepsilon_p/\varepsilon_f < 1$ or (d) $\varepsilon_p/\varepsilon_f > 1$. Electrical stress and electric field vectors on outer and inner side of membrane are shown by red and blue arrows, respectively. . (For interpretation of the references to color in this figure legend, the reader is referred to the web version of this article.)

jump condition is as follow.

$$[\beta U_n] - V = \beta^+ U_n^+ - \beta^- U_n^- - V \tag{14}$$

where U_n is the discrete form of $\partial u/\partial n$ and V is discrete values of v. In other word, this relation should be satisfied at each control points. Interpolation is required to calculate U_n in each control point. For this purpose, the weighted least squares interpolation method is used. Therefore, the approximate interpolation U_n^- is calculated as

$$\frac{\partial U^-}{\partial n}(X) = \sum_{k=0}^{k_s-1} \gamma_k U_{i^*+i_k j^*+j_k} - C \tag{15}$$

where C is a correction term. Using Taylor series and minimizing the local truncation error, we can get the following equations system

$$\begin{aligned} &a_1 + a_2 = 0 \\ &a_3 + a_4 = 1 \\ &a_5 + a_6 = 0 \\ &a_7 + a_8 = 0 \\ &a_9 + a_{10} = 0 \\ &a_{11} + a_{12} = 0 \end{aligned} \tag{16}$$

Then, the coefficients $\{\gamma_k\}$ can be determined from Eq. (16). If this system is underdetermined, the singular value decomposition (SVD i.e. an approach to solving underdetermined system of equations) is used to solve it. Finally, by using weighted least square interpolation, the discrete form of jump conditions can be obtained as below

$$\begin{aligned} &\left(\beta^+ - \beta^-\right) \sum_{k=0}^{k_s-1} \gamma_k U_{i^*+i_k j^*+j_k} + \left(\beta^+ - \left(\beta^+ - \beta^-\right)\right. \\ &\quad \left. \times \left(a_4 + a_8 \chi'' - a_{10} \chi''\right)\right) g - \left(\beta^+ - \beta^-\right) a_{12} g' \\ &\quad -\nu - \left(\beta^+ - \beta^-\right) \overline{C} \cong 0 \end{aligned} \tag{17}$$

where $\overline{C}$ is expressed as

$$\overline{C} = a_2 \omega + a_6 \omega' - a_8 \left(\omega'' - \left[\frac{f}{\beta}\right]\right) + a_{10} \omega'' + a_{12} \omega' \chi'' \tag{18}$$

As a result, the matrix form of Eq. (14) is expressed as

$$EU + TG = PV + QW \tag{19}$$

Thus, with solving Eqs. (13) and (19), we can get the final solutions for the proposed problem in Eqs. (1) and (2).

Discrete form of Eq. (1) using five-point central finite difference stencil can be obtained as

$$\frac{1}{h^2}\left(\phi_{i+1,j} + \phi_{1-1,j} - 4\phi_{i,j} + \phi_{i,j+1} + \phi_{i,j-1}\right) = C_{ij} \tag{20}$$

where C_{ij} is the correction term and ϕ is the discrete form of φ. By defining augmented variable as

$$\frac{\partial \varphi_p}{\partial \overline{n}} - \frac{\partial \varphi_f}{\partial \overline{n}} = g\,(\eta) \tag{21}$$

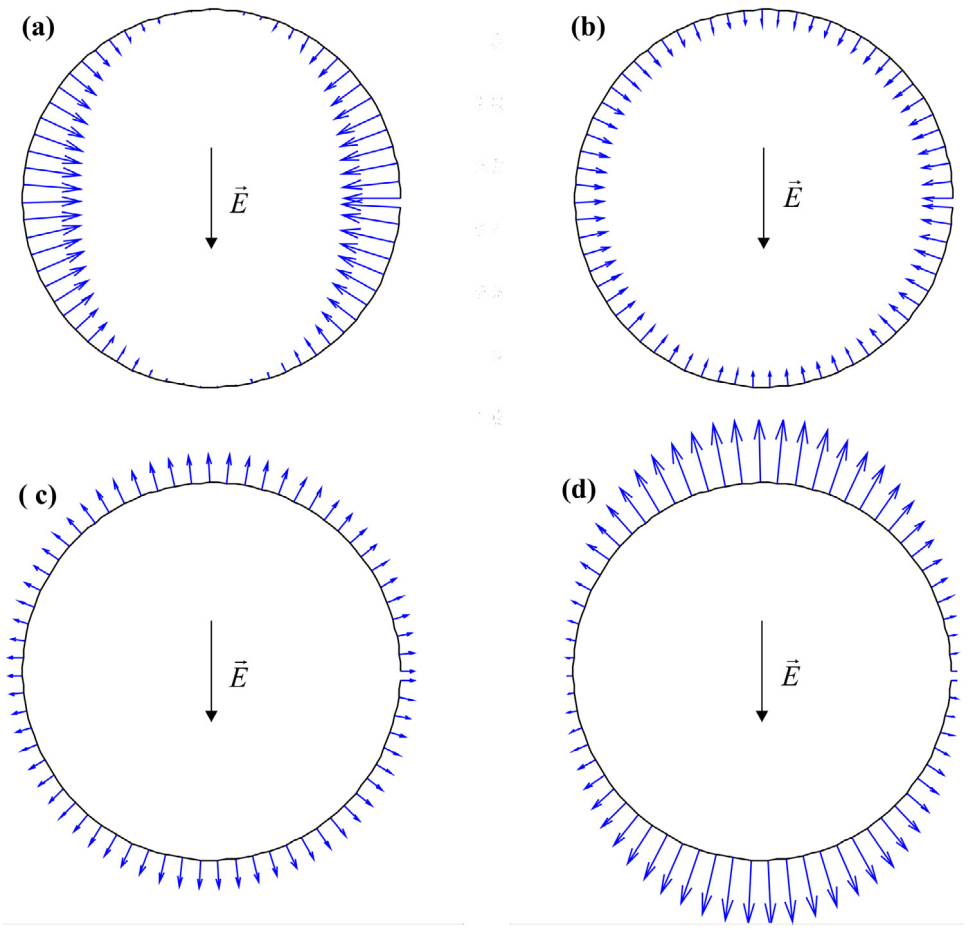

Fig. 6. Total electrical stresses acted on cell surface for different permittivity ratio (a) $\varepsilon_p/\varepsilon_f = 0.01$, (b) $\varepsilon_p/\varepsilon_f = 0.5$, (c) $\varepsilon_p/\varepsilon_f = 2$ and (d) $\varepsilon_p/\varepsilon_f = 10$.

where discrete form g is as G the matrix form of Eq. (20) can be expressed as Eq. (22).

$$A\phi + BG = F_1 \tag{22}$$

Discrete form of jump conditions also is expressed as Eq. (23).

$$\begin{aligned}&\left(\varepsilon_f - \varepsilon_p\right)\sum_{k=0}^{k_s-1}\gamma_k\phi_{i^*+i_k,j^*+j_k} + \left(\varepsilon_f - \left(\varepsilon_f - \varepsilon_p\right)\right.\\ &\quad\times\left.\left(a_4 + a_8\chi'' - a_{10}\chi''\right)\right)g\\ &\quad-\left(\varepsilon_f - \varepsilon_p\right)a_{12}g' - \left(\varepsilon_f - \varepsilon_p\right)\overline{C} \cong 0\end{aligned} \tag{23}$$

where $\overline{C}$ is calculated from Eq. (18) and γ_k coefficients are calculated from solving Eq. (16). The matrix form of Eq. (23) can be written as

$$E\phi + TG = F_2 \tag{24}$$

Finally, the matrix form of electrostatic equations can be obtained as

$$\begin{bmatrix} A & B \\ E & T \end{bmatrix}\begin{bmatrix} \phi \\ G \end{bmatrix} = \begin{bmatrix} F_1 \\ F_2 \end{bmatrix} \tag{25}$$

It is not possible to express a closed form for matrices E, T, B, F_1 and F_2 explicitly. The matrices must be calculated element by element by solving the system of linear equations of Eq. (16) for each control point.

4. Results and discussion

Convergence analysis was carried out first for the numerical solutions from fast IIM. To examine this issue, the problem has been solved with different mesh sizes and the results are presented in Fig. 2, in which the electrostatic potential at the line $x = 25$ μm is described. It should be noted that the number of control points and the number of points used for interpolation are also important for the convergence of fast IIM. In the calculation, the number of points for the interpolation is 16 and the number of control points on cell boundary is selected according to the mesh size. The segments on cell boundary should be almost the size of mesh. It can be seen from Fig. 2(a) and (b) that using mesh size $h = 0.6$ for $\varepsilon_p/\varepsilon_f = 0.01$ and mesh size $h = 0.8$ for $\varepsilon_p/\varepsilon_f = 10$, the convergence for the results can be secured. As shown in the figures, the electric potential on the boundary of cell is continuous but the electric field, i.e., the gradient of electrostatic potential, is discontinuous. This discontinuity leads to electrical stresses over cell surface.

To verify the accuracy of numerical algorithm, we compare the dielectrophoresis force calculated by integration of the electrical stresses over cell surface and the force obtained by effective dipole moment (EDM) approximation. In the latter approach, the cell is replaced by a point dipole or multipole moment. It is accurate when the cell size is negligible compared with the size of electric field nonuniformity. Thus, in this method the changes in electrostatic potential distribution induced by cell are not taken into account.

When a 2D dielectric cell with permittivity of ε_p, without ohmic loss, is immersed in a dielectric fluid with permittivity of ε_f and exposed to a non-uniform DC electric field, for the domain geometry with $a = 50\mu$m as shown in Fig. 1, and the boundary

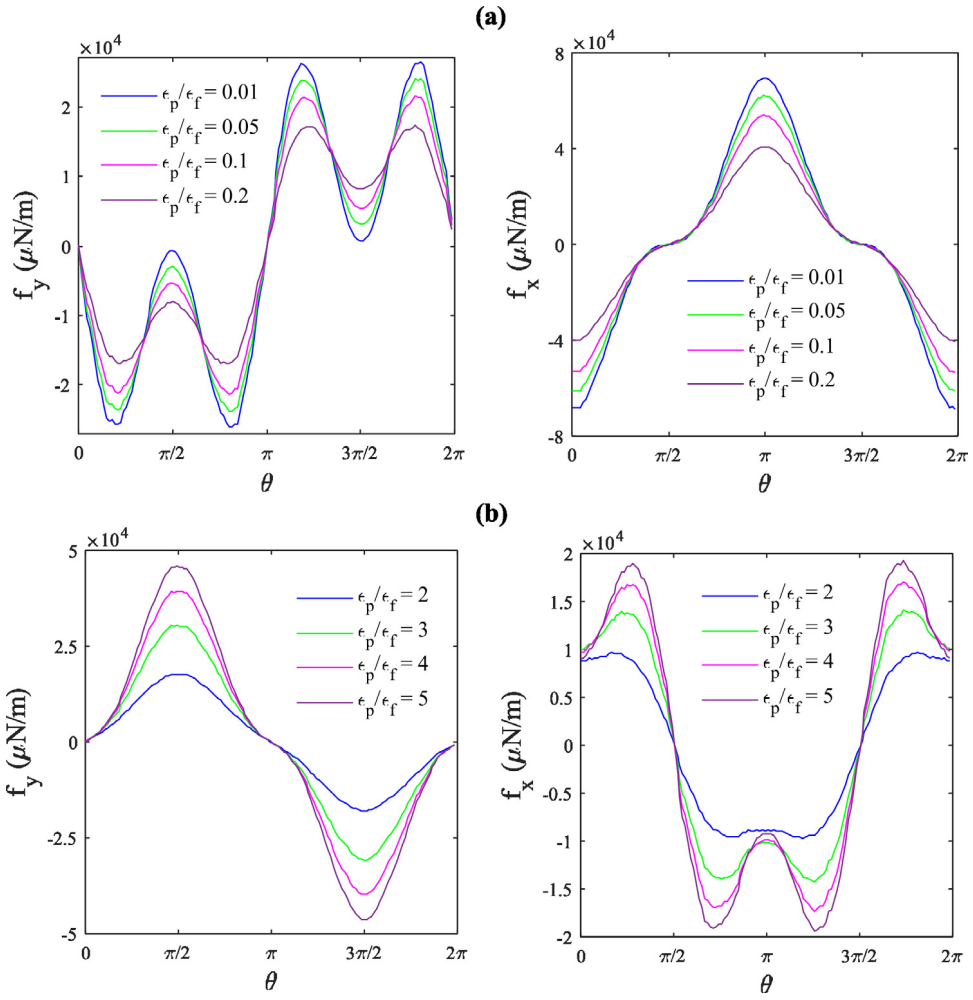

Fig. 7. The y and x-components of total electrical stresses (μN/m) generated over cell surface with permittivity ratio (a) $\varepsilon_p/\varepsilon_f < 1$ and (b) $\varepsilon_p/\varepsilon_f > 1$.

conditions are expressed as [50]

$$\begin{aligned} &\varphi = 10^9 y^2 && at\ x = 0 \\ &\varphi = 10^9\left(y^2 - a^2\right) && at\ x = a \\ &\varphi = 10^9 x^2 && at\ y = 0 \\ &\varphi = 10^9\left(a^2 - x^2\right) && at\ y = a \end{aligned} \tag{26}$$

Then, the DEP force is calculated by Eq. (27) with considering the effective dipole moment approximation [41]

$$\begin{aligned} f_x &= 2C\left(\frac{\partial\varphi}{\partial x}\frac{\partial^2\varphi}{\partial x^2} + \frac{\partial\varphi}{\partial y}\frac{\partial^2\varphi}{\partial x\partial y}\right) \\ f_y &= 2C\left(\frac{\partial\varphi}{\partial x}\frac{\partial^2\varphi}{\partial x\partial y} + \frac{\partial\varphi}{\partial y}\frac{\partial^2\varphi}{\partial y^2}\right) \end{aligned} \tag{27}$$

where C is expressed as

$$C = \pi\varepsilon_f\frac{\varepsilon_p - \varepsilon_f}{\varepsilon_p + \varepsilon_f}R^3 \tag{28}$$

The x and y-components of resultant DEP force calculated by both approaches versus the cell radius is presented in Fig. 3(a) and (b) for a cell with permittivity ratio $\varepsilon_p/\varepsilon_f < 1$ and $\varepsilon_p/\varepsilon_f > 1$, respectively. As shown in Fig. 3, the difference of results from the two methods increases as cell radius increases. When the cell size is negligible compared with the dimensions of the channel, the EDM method can give satisfying accuracy. Therefore, the negligible difference between DEP resultant force is obtained from both approaches when the cell radius is smaller than 4 μm, which shows that the numerical solution is accurate.

The electrical potential and electrical field distribution are strongly affected by the cell and its relative permittivity compared with the surrounding fluid. Fig. 4(a) and (b) shows the electrostatic potential and electric field distribution without the presence of cell, respectively, which are uniformly distributed. However, when the dielectric lossless cell with permittivity of ε_p immersed in a dielectric fluid with permittivity of ε_f is exposed to a uniform DC electric field, if the cell has greater electric permittivity that the insulating suspension fluid, the distributions for both potential and electric fields are distorted due to the mismatch of the permittivity between fluid and cell, as shown in Fig. 4(c) and (d). On the other hand, if the cell has a smaller electrical permittivity than the fluid, different distributions for potential and electric fields will be generated (Fig. 4(e) and (f)). The behavior of these two kinds of cells is different in electric field and is expected to generate the different stress distributions on the surface of the cell.

It is obvious that the electrostatic potential is continuous on cell surface while the electric field (gradient of electric field) is discontinuous on the cell boundary. According to the Gauss law, polarized bound charge is induced at the cell/liquid interface by the applied DC field (no free charge component due to zero conduction effect), and as a consequence, electrical stress is generated on the surface of the cell. These tensions can be

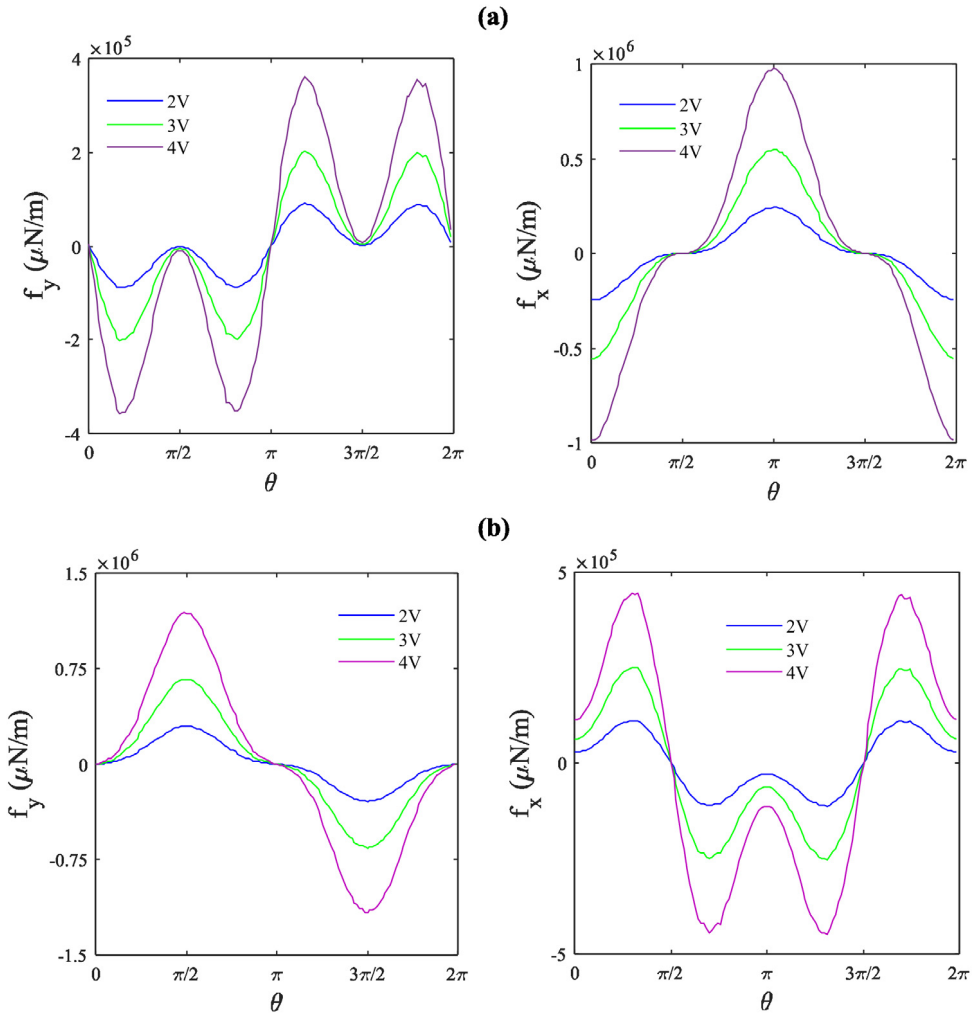

Fig. 8. Effect of applied DC voltage on electrical stresses (μN/m) generated on cell surface. Cell permittivity ratio is (a) $\varepsilon_p/\varepsilon_f = 0.01$ and (b) $\varepsilon_p/\varepsilon_f = 10$ and call radius is $R = 5$ μm.

calculated using MST (Maxwell stress tensor) method. The total stress is a combination of internal and external electrical tensions. Integration of the total stress along the boundary of the cell obtains the dielectrophoresis force applied on cell. To examine the electrical stresses applied on the cell surface, Maxwell stress tensor on the boundary of the cell must be calculated based on the electric field on the boundary of the cell. Thus, the electric field and its discontinuity must be exactly calculated on cell boundary. The key advantage of the immersed interface method in this research, is that it can help us to handle the discontinuities of solution accurately. Fig. 5(a) and (b) shows the electric field vectors on inner and outer surface of the cell membrane for different dielectric properties of $\varepsilon_p/\varepsilon_f < 1$ and $\varepsilon_p/\varepsilon_f > 1$. The discontinuity of the electric field is clearly observable in this figure. Fig. 5(c) and (d) presents the internal and external electrical stress distribution for cell with permittivity ratio $\varepsilon_p/\varepsilon_f < 1$ and $\varepsilon_p/\varepsilon_f > 1$, respectively. Maxwell stress tensor is calculated by solving the governing electrostatic equations by fast IIM and interpolating the electric field on the surface of the cell.

The total or resultant stresses of the internal and external tensions applied on the surface of cells with different permittivity are shown in Fig. 6. It can be seen that for the cells with very small permittivity, e.g. $\varepsilon_p/\varepsilon_f = 0.01$, the total stress is mainly compressive, and it reaches its largest values at the perpendicular direction of electric field, as shown in Fig. 6(a) and (b). With the increase of the permittivity of cell, $\varepsilon_p/\varepsilon_f$, the compressive stress decreases in all directions and electrical stresses are more uniformly distributed over cell surface. When $\varepsilon_p/\varepsilon_f > 1$, however, the total stresses acted on the cell becomes tensile along the whole surface of the cell in Fig. 6(c) and (d). If the permittivity of cell is much larger than 1, then we see the maximum tensile stress becomes along the electric field direction.

Fig. 7(a) and (b) presents the x and y components of total electrical stresses generated on the surface of cell with $\varepsilon_p/\varepsilon_f < 1$ and $\varepsilon_p/\varepsilon_f > 1$, respectively. As it can be seen from the figures, by increasing or decreasing the ratio $\varepsilon_p/\varepsilon_f$ from 1, the electrical stresses acted on the cell surface becomes significant. This means the larger force generated on cell surface when larger mismatched permittivity happens between the cell and surrounded fluid. Fig. 8 shows the effect of applied DC voltage on surface electrical stresses generated on a cell with $\varepsilon_p/\varepsilon_f < 1$ and $\varepsilon_p/\varepsilon_f > 1$, respectively. It is obvious that increased applied voltage results in larger stresses generated on cell surface. Fig. 8. shows the second order voltage dependence of electrical stresses acting on cell surface, which is due to the field-induced feature of the interfacial charge. Thus, the stresses can be tuned by either applying a higher electric field or by changing the cell environment (surrounding fluid) if the cell is determined.

5. Conclusion

In this study, we have numerically investigated the interaction of a protoplast cell and electric field. The governing PDEs

equations are solved by fast IIM method with interfaces and irregular domains involved. Results showed that the presence of cell would distort the local distribution of electric potential and electric field, and these changes were dependent on the relative permittivity between cell and insulating suspension fluid. The distribution of electrical stresses acted over the cell surface was calculated by Maxwell stress tensor. It was shown that, mismatched permittivity between cell and insulating suspension fluid was essential for generating and tuning the total stresses exerted on cell surfaces except the applied voltage. This study offers approaches to analytically study formation of hydrophilic pores in cell membrane under an electric field and electroporation phenomenon. This research may also be helpful in explaining the mechanism of cells rupture and can be used for theoretical study of the mechanical properties of cells by putting them in an electric field. Studying the stresses acting on cells and living organisms is very essential in other fields of biotechnology such as stem cell and proteomic studies. For example, when a stem cell undergoes stresses, it differentiates into a variety of different tissues, and the stresses can be either applied mechanically — like applying hydrostatic pressure or electrically. Therefore, it is important to exactly investigate these electrical stresses. In the future work, to further improve the results, more exact electrical model for cells and suspension fluid can be considered to study the behaviors of a single cell in more realistic culture media and its plasma membrane structural changes in the presence of an electric field.

Acknowledgments

The work was supported by Iran National Science Foundation. The work was also partially supported by the Startup fund from the School of Packaging at Michigan State University, USA.

References

[1] P. Cahan, H. Li, S.A. Morris, E.L. da Rocha, G.Q. Daley, J.J. Collins, CellNet: network biology applied to stem cell engineering, Cell 158 (2014) 903–915.
[2] Q. Deng, D. Ramsköld, B. Reinius, R. Sandberg, Single-cell RNA-seq reveals dynamic, random monoallelic gene expression in mammalian cells, Scienc 343 (2014) 193–196.
[3] X. Ding, M.P. Stewart, A. Sharei, J.C. Weaver, R.S. Langer, K.F. Jensen, High-throughput nuclear delivery and rapid expression of DNA via mechanical and electrical cell-membrane disruption, Nature Biomed. Eng. 1 (2017) 0039.
[4] P.D. Hsu, E.S. Lander, F. Zhang, Development and applications of CRISPR-Cas9 for genome engineering, Cell 157 (2014) 1262–1278.
[5] B. McKinley, W. Rooney, C. Wilkerson, J. Mullet, Dynamics of biomass partitioning, stem gene expression, cell wall biosynthesis, and sucrose accumulation during development of Sorghum bicolor, Plant J. 88 (2016) 662–680.
[6] L.S. Qi, M.H. Larson, L.A. Gilbert, J.A. Doudna, J.S. Weissman, A.P. Arkin, W.A. Lim, Repurposing CRISPR as an RNA-guided platform for sequence-specific control of gene expression, Cell 152 (2013) 1173–1183.
[7] Y. Rajendra, G. Barnard, 2016. High titer transient gene expression platform based on GS CHO cell line–rapid protein expression tool for preclinical drug development.
[8] E. Zlotorynski, Genome engineering: NHEJ and CRISPR-Cas9 improve gene therapy, Nature Rev. Mol. Cell Biol. 18 (2017) 4-4.
[9] D. Dupéré-Richer, M. Kinal, F. Pettersson, A. Emond, M.N. Calvo-Vidal, J.N. Nichol, C. Guilbert, D. Plourde, K. Klein Oros, T.H. Nielsen, Increased protein processing gene signature in HDACi-resistant cells predicts response to proteasome inhibitors, Leuk. & Lymphoma 58 (2017) 218–221.
[10] R.L. Harrison, D.L. Jarvis, Transforming lepidopteran insect cells for improved protein processing and expression, in: Baculovirus and Insect Cell Expression Protocols, 2016, pp. 359–379.
[11] N. Iyer, T. Wilems, S. Sakiyama-Elbert, S. Ding, P. Kingshott, H. Thissen, M. Pera, P. Wang, Biocatalysis, protein engineering and nanobiotechnology, in: Biotechnology and Bioengineering, 2017, p. 114.
[12] J.J. Milne, Scale-up of protein purification: downstream processing issues, in: Protein Chromatography: Methods and Protocols, 2017, pp. 71–84.
[13] M.A. Kalwat, C. Wichaidit, A.Y. Nava Garcia, M.K. McCoy, K. McGlynn, I.H. Hwang, J.B. MacMillan, B.A. Posner, M.H. Cobb, Insulin promoter-driven Gaussia Luciferase-Based Insulin Secretion Biosensor Assay for discovery of β-cell glucose-sensing pathways, ACS sensors 1 (2016) 1208–1212.
[14] M.A. Kalwat, C. Wichaidit, A.Y. Nava Garcia, M.K. McCoy, K. McGlynn, I.H. Hwang, J.B. MacMillan, B.A. Posner, M.H. Cobb, Correction to insulin promoter-driven Gaussia Luciferase-Based Insulin Secretion Biosensor Assay for discovery of β-cell glucose-sensing pathways, ACS Sensors 2 (2017) 316-316.
[15] S. Merfeld-Clauss, B.R. Lease, H. Lu, K.L. March, D.O. Traktuev, Adipose stromal cells differentiation toward smooth muscle cell phenotype diminishes their vasculogenic activity due to induction of activin A secretion, J. Tissue Eng. Regen. Med. (2016).
[16] Y. Fan, H.F. Kildegaard, M.R. Andersen, Trends and approaches in n-glycosylation engineering in chinese hamster ovary cell culture, in: 11th Danish Conference on Biotechnology and Molecular Biology, 2016.
[17] C. Shurer, M. Paszek, Abstract A59: Glycosylation Dynamically Tunes the Biophysical Properties of the Cancer Cell Glycocalyx, AACR, 2017.
[18] S.J. Karnik, D. Robinson, Stem cell proliferation and differentiation through capped clay nanotubes, FASEB J. 30 (2016) 91.91-91.91.
[19] T. Liu, R. Huang, J. Zhong, Y. Yang, Z. Tan, W. Tan, Control of cell proliferation in E-jet 3D-printed scaffolds for tissue engineering applications: influence of cell alignment angle, J. Mater. Chem. B (2017a).
[20] J. Vaca-González, J. Guevara, J. Vega, D. Garzón-Alvarado, An in vitro chondrocyte electrical stimulation framework: a methodology to calculate electric fields and modulate proliferation, cell death and glycosaminoglycan synthesis, Cell. Mol. Bioeng. 9 (2016) 116–126.
[21] E.R. Wagner, Future of Soft Tissue Regeneration: 3D Printed PCLF Scaffolds, Progenitor Cell Proliferation and Differentiation, and Vascularization with Tissue Infiltration, College of Medicine-Mayo Clinic, 2016.
[22] T. Kotnik, W. Frey, M. Sack, S.Haberl. Meglič, M. Peterka, D. Miklavčič, Electroporation- based applications in biotechnology. 0000. Trends in Biotechnology 33, 480-488.
[23] H. Leontiadou, A.E. Mark, S.J. Marrink, Molecular dynamics simulations of hydrophilic pores in lipid bilayers, Biophys. J. 86 (2004) 2156–2164.
[24] A. Barnett, J.C. Weaver, Electroporation: a unified, quantitative theory of reversible electrical breakdown and mechanical rupture in artificial planar bilayer membranes, J. Electroanal. Chem. Interfacial Electrochem. 320 (1991) 163–182.
[25] S.A. Freeman, M.A. Wang, J.C. Weaver, Theory of electroporation of planar bilayer membranes: predictions of the aqueous area, change in capacitance, and pore-pore separation, Biophys. J. 67 (1994) 42–56.
[26] J.C. Weaver, A. Barnett, Progress toward a theoretical model for electroporation mechanism: membrane electrical behavior and molecular transport, in: Guide to Electroporation and Electrofusion, 1992, pp. 91–117.
[27] G. Pucihar, T. Kotnik, D. Miklavčič, J. Teissié, Kinetics of transmembrane transport of small molecules into electropermeabilized cells, Biophys. J. 95 (2008) 2837–2848.
[28] M. Kandušer, D. Miklavčič, Electroporation in Biological Cell and Tissue: An Overview, Electrotechnologies for Extraction from Food Plants and Biomaterials, Springer, 2009, pp. 1–37.
[29] S. Priya, V. Gowrisree, Modeling of electroporation and electric field investigation for a single cell dispersed in liquid foods, Indian J. Sci. Technol. 7 (2014) 104–113.
[30] E. Tekle, R. Astumian, W. Friauf, P. Chock, Asymmetric pore distribution and loss of membrane lipid in electroporated DOPC vesicles, Biophys. J. 81 (2001) 960–968.
[31] G. Bryant, J. Wolfe, Electromechanical stresses produced in the plasma membranes of suspended cells by applied electric fields, J. Membr. Biol. 96 (1987) 129–139.
[32] D. Needham, R. Hochmuth, Electro-mechanical permeabilization of lipid vesicles. role of membrane tension and compressibility, Biophys. J. 55 (1989) 1001–1009.
[33] D.P. Tieleman, H. Leontiadou, A.E. Mark, S.-J. Marrink, Simulation of pore formation in lipid bilayers by mechanical stress and electric fields, J. Am. Chem. Soc. 125 (2003) 6382–6383.
[34] J. Akinlaja, F. Sachs, The breakdown of cell membranes by electrical and mechanical stress, Biophys. J. 75 (1998) 247–254.
[35] M. Schmeer, T. Seipp, U. Pliquett, S. Kakorin, E. Neumann, Mechanism for the conductivity changes caused by membrane electroporation of CHO cell-pellets, Phys. Chem. Chem. Phys. 6 (2004) 5564–5574.
[36] T. Griese, S. Kakorin, E. Neumann, Conductometric and electrooptic relaxation spectrometry of lipid vesicle electroporation at high fields, Phys. Chem. Chem. Phys. 4 (2002) 1217–1227.
[37] C.A. Jordan, E. Neumann, A.E. Sowers, Electroporation and Electrofusion in Cell Biology, Springer Science & Business Media, 2013.
[38] I.I. Hosseini, M. Moghimi Zand, Optimized Microstructure for Single Cell Trapping Utilizing Contactless Dielectrophoresis, 2017.
[39] W. Liu, Y. Ren, Y. Tao, X. Chen, B. Yao, M. Hui, L. Bai, Control of two-phase flow in microfluidics using out-of-phase electroconvective streaming, Phys. Fluids 29 (2017b) 112002.

[40] T.B. Jones, Electromechanics of Particles, Cambridge University Press, 2005.
[41] C. Xie, B. Chen, C.-O. Ng, X. Zhou, J. Wu, Numerical study of interactive motion of dielectrophoretic particles, Eur. J. Mech. B Fluids 49 (2015) 208–216.
[42] Y. Jia, Y. Ren, W. Liu, L. Hou, Y. Tao, Q. Hu, H. Jiang, Electrocoalescence of paired droplets encapsulated in double-emulsion drops, Lab Chip 16 (2016) 4313–4318.
[43] W. Liu, Y. Ren, Y. Tao, Y. Li, X. Chen, Controllable rotating behavior of individual dielectric microrod in a rotating electric field, Electrophoresis 38 (2017c) 1427–1433.
[44] W. Liu, J. Shao, Y. Jia, Y. Tao, Y. Ding, H. Jiang, Y. Ren, Trapping and chaining self-assembly of colloidal polystyrene particles over a floating electrode by using combined induced-charge electroosmosis and attractive dipole–dipole interactions, Soft Matter 11 (2015) 8105–8112.
[45] M. Sussman, P. Smereka, S. Osher, A level set approach for computing solutions to incompressible two-phase flow, J. Comput. Phys. 114 (1994) 146–159.
[46] G.R. Shubin, J.B. Bell, An analysis of the grid orientation effect in numerical simulation of miscible displacement, Comput. Methods Appl. Mech. Engrg. 47 (1984) 47–71.
[47] C.S. Peskin, The immersed boundary method, Acta Numer. 11 (2002) 479–517.
[48] Z. Li, K. Ito, The Immersed Interface Method: Numerical Solutions of PDEs Involving Interfaces and Irregular Domains, Siam, 2006.
[49] R.J. Leveque, Z. Li, The immersed interface method for elliptic equations with discontinuous coefficients and singular sources, SIAM J. Numer. Anal. 31 (1994) 1019–1044.
[50] K. Dastani, M. Moghimi Zand, A. Hadi, Dielectrophoretic effect of nonuniform electric fields on the protoplast cell, J. Comput. Appl. Mech. 48 (2017) 1–14.